

1  
2  
3  
4  
5  
6  
7  
8  
9  
10  
11  
12  
13  
14  
15  
16  
17  
18  
19

**Erosion monitoring during core overtopping using a laboratory model with  
digital image correlation and X-ray microcomputed tomography**

by

Kevin Dumberry<sup>1,2</sup>, François Duhaime<sup>1,3</sup>, Yannic A. Ethier<sup>1,4</sup>

Submitted for publication to the

**Canadian Geotechnical Journal**

June 2017

<sup>1</sup> Department of Construction Engineering, École de technologie supérieure, 1100, rue Notre-Dame  
Ouest, Montréal, Québec, Canada, H3C 1K3

<sup>2</sup> Email: kevin.dumberry.1@ens.etsmtl.ca

<sup>3</sup> Corresponding author: François Duhaime (email: francois.duhaime@etsmtl.ca)

<sup>4</sup> Email: yannic.ethier@etsmtl.ca

## 20 **Abstract**

21 Core overtopping in embankment dams is an important phenomenon that may lead to contact erosion  
22 along the core/filter interface. This paper presents new experimental results regarding erosion  
23 mechanisms at the core/filter interface during core overtopping. The experimental results were obtained  
24 using a reduced-scale model with a variable upstream water level. Digital image correlation (DIC),  
25 microcomputed tomography ( $\mu$ CT) and sediment collection at the outlet were used to quantify erosion.  
26 Four experimental runs were conducted with a till core and different filters. Only one of the four filters  
27 satisfied the filter criteria that were applied. No contact erosion occurred during this test. For filters that  
28 did not respect the filter criteria, piping occurred within the core along the downstream slope when the  
29 water level reached the top of the core. As a result of the self-healing process within the core material, the  
30 erosion rate decayed with time as the hydraulic gradient increased. Results for DIC mainly reflected  
31 settlements within the filter due to erosion and a soil arching effect. The magnitude of the displacement  
32 vector obtained with DIC is directly proportional to the volume of till eroded.  $\mu$ CT showed that contact  
33 erosion occurred continuously.

34 **Keywords:** core overtopping, contact erosion, embankment dams, digital image correlation,  
35 microcomputed tomography

36

## 37 **Résumé**

38 Pour les barrages en remblai zonés, le franchissement de noyau est un problème important qui peut  
39 provoquer une érosion de contact le long de l'interface noyau/filtre. Cet article présente de nouveaux  
40 résultats expérimentaux sur les mécanismes d'érosion à l'interface noyau/filtre durant le franchissement  
41 de noyau. Les résultats expérimentaux ont été obtenus à partir d'un modèle à échelle réduite dont le  
42 niveau d'eau amont est variable. La corrélation d'images numériques (DIC), la microtomodensitométrie à  
43 rayons X ( $\mu$ CT) et la collecte de sédiments en aval du montage ont permis de quantifier l'érosion. Quatre  
44 essais ont été effectués avec un noyau en till et différents matériaux filtrants. Seulement un des filtres  
45 respectait les critères de filtre qui ont été utilisés. Aucune érosion de contact ne s'est produite pour ce test.  
46 Pour les filtres qui ne respectaient pas les critères de filtre, un phénomène d'érosion régressive (renard  
47 hydraulique) est apparu le long de la pente aval du noyau lorsque le niveau d'eau a atteint le sommet du  
48 noyau. Le taux d'érosion a diminué dans le temps à mesure que le gradient hydraulique augmentait, dû à  
49 un phénomène d'auto-réparation du noyau. La DIC a permis de mettre en évidence les tassements  
50 verticaux dans le filtre ainsi qu'un effet d'arche. Le déplacement vectoriel mesuré par la DIC est  
51 directement proportionnel au volume de till érodé. La  $\mu$ CT a démontré que l'érosion de contact se produit  
52 en continu.

53 **Mots clés** : franchissement de noyau, érosion de contact, barrages en remblai, corrélation d'images  
54 numériques, microtomodensitométrie

55

56 **List of symbols**

57	$A$	Modified fines content
58	$C_u$	Coefficient of uniformity
59	$D_{10}$	Effective diameter
60	$D_{15}$	Diameter of filter particles corresponding to 15% passing by mass
61	$d_{85}$	Diameter of core particles corresponding to 85% passing by mass
62	$e$	Void ratio
63	$e_{\min}$	Minimum-index void ratio
64	$e_{\max}$	Maximum-index void ratio
65	$G_s$	Specific gravity of solids
66	$I_d$	Relative density index
67	$RC$	Relative compaction
68	$w$	Water content
69	$w_{\text{opt}}$	Optimum water content
70	$\rho_d$	Dry density
71	$\rho_{d \max}$	Maximum dry density
72	$\rho_{d \min}$	Minimum dry density

73

## 74 **Introduction**

75           The core/filter interface of an embankment dam can be vulnerable to erosion if the upstream  
76 water level rises over the top of the core (Figure 1). In the long term, instabilities can be generated and  
77 filter effectiveness within the dam reduced. This phenomenon, called core overtopping, may be a  
78 consequence of heavy precipitation, climate change or inadequate spillway capacity. Due to recent  
79 improvements in the analysis of extreme flood events, and better precipitation and watershed information,  
80 it has been inferred that several thousand dams in the United States alone do not have sufficient spillway  
81 capacity to accommodate the appropriate design floods (FEMA 2014).

82           Dam failure can have severe economic, social and environmental consequences. Since internal  
83 erosion is recognized as an important cause of dam failure (Foster et al. 2000), the ability to predict and  
84 understand erosion processes for different parts of a dam is fundamental. In the complex setting of an  
85 embankment dam crest, previous studies suggest that erosion is mostly associated with: 1) large hydraulic  
86 gradients and flow velocities, especially at the downstream edge of the core/filter interface (Wörman and  
87 Skoglund 1992) and in the unsaturated portion of the core and filter (Zhang and Chen 2006); 2) within  
88 zones of low effective stress due to soil arching (Fell et al. 2015). Internal erosion is also associated with  
89 materials that are internally unstable (broadly or gap-graded grain size distributions) or combinations of  
90 materials that fail to satisfy the filter criteria (e.g., Sherard et al. 1984; Indraratna et al. 2011). Currently,  
91 the design of filters and the prediction of their long-term behaviour are mainly assessed by empirical  
92 relationships based on grain size distributions and judgment (Fell et al. 2015). These criteria have evolved  
93 through time. As a result, older structures do not necessarily reflect current practices for filter design and  
94 could be susceptible to erosion.

95           A limited number of experimental studies have addressed the phenomenon of core overtopping.  
96 Some researchers focused on the horizontal interface between a base material and a coarse material under  
97 tangential flow conditions (Wörman 1996; Guidoux et al. 2010; Dionne and Konrad 2015), while others  
98 considered more realistic geometric configurations and hydraulic boundaries (Wörman and Olafsdottir

99 1992; Wörman and Skoglund 1992; Seo et al. 2006; Maknoon and Mahdi 2010). Most experimental  
100 studies have shown that fulfilling the filter criteria prevents the propagation of contact erosion during core  
101 overtopping. Otherwise, contact erosion is initiated at the downstream edge of the core/filter interface,  
102 where local hydraulic gradients are higher. Since these local hydraulic gradients do not increase  
103 significantly with the rise of the upstream water level, the progression of contact erosion is not influenced  
104 by an increasing water level (Wörman and Olafsdottir 1992).

105 Empirical criteria based solely on grain size distributions are not sufficient to model the  
106 progression of erosion. Internal erosion depends on pore and grain geometries, effective stress, porosity,  
107 water velocity and degree of saturation. The interplay between these parameters has also been  
108 demonstrated for other erosion phenomena, such as piping, where a granular material is eroded through a  
109 conduit (Richards and Reddy 2012; Van Beek et al. 2015), and bridge scour (Briaud 2008). For instance,  
110 Richards and Reddy (2012) observed that seepage velocities between 0.02 and 1.2 cm/s were needed to  
111 initiate piping in different soils depending on the effective stress, the void ratio and the grain size  
112 distribution. Low velocities were sufficient to initiate internal erosion (suffusion) for soils with non-  
113 plastic fines. For bridge scour, Briaud (2008) showed that a velocity in excess of 10 cm/s is needed to  
114 erode fine sand.

115 The parameters that control erosion depend on both macro- and microscale phenomena (Pirnia et  
116 al. 2016). State-of-the-art experimental and numerical methods, such as X-ray microcomputed  
117 tomography ( $\mu$ CT), digital image correlation (DIC) and discrete element modelling (DEM), now allow  
118 the microscale behaviour of soil to be studied. However, the progression of internal erosion at the pore  
119 scale has not been studied thoroughly (Binner et al. 2010; Beguin et al. 2013; Takano et al. 2015). Most  
120 studies used  $\mu$ CT to evaluate the properties of uniform granular specimens, such as bulk density, water  
121 content and porosity (Tollner and Verma 1989; Kim et al. 2013, Takano et al. 2015). DIC has been  
122 predominantly used to investigate local strains in granular materials under loading (White et al. 2003; Pan  
123 et al. 2007; Boccalini et al. 2015).

124           There is currently a lack of knowledge regarding the progression of contact erosion for complex  
125 geometries, flow conditions influenced by gravity, upstream hydraulic boundaries that vary in the short-  
126 term and broadly graded materials. Indeed, a review of the literature indicates that there is a need for  
127 experimental data that are more consistent with actual field conditions. Moreover, few attempts have been  
128 made to examine contact erosion with DIC and  $\mu$ CT. This study aims at evaluating the relationship  
129 between the progression of erosion during core overtopping and filter criteria. It is inferred that a  
130 laboratory model more representative of actual field conditions along with DIC and  $\mu$ CT should provide  
131 insight on the erosion mechanisms at the local scale during core overtopping. The experimental setup  
132 allows the placement of broadly graded materials with a representative geometry and the application of  
133 2D hydraulic boundary conditions. This paper describes the physical model developed for this study.  
134 Important DIC and  $\mu$ CT concepts are also defined. Experimental results are presented, along with a  
135 discussion that puts the emphasis on the conditions leading to erosion and the potential applications of  
136 DIC and  $\mu$ CT in the study of internal and contact erosion.

137

## 138 **Methodology**

### 139 **Experimental Setup**

140           The experimental setup used in this study is presented in Figure 2. The basin is made of 19-mm-  
141 thick transparent acrylic to allow the erosion process to be seen during the tests. The basin contains an  
142 upstream water reservoir connected to the main section where the till and filter materials are placed. The  
143 main section is 1.0 m long, 0.5 m wide and 0.6 m high, with a total volume of 0.3 m<sup>3</sup>. The model width  
144 was chosen to have a ratio of at least 1:8 between the maximum particle size of the tested materials and  
145 the basin dimensions (Figure 2a). This requirement limits the influence of preferential flow, erosion and  
146 segregation along the walls of the test setup (Chapuis 2012). In accordance with this maximum ratio, the  
147 maximum particle size was 56 mm.

148           The physical model represents the top of an embankment dam core. The core material forms a  
149 trapezoidal prism with a height of 0.25 m, a base of 0.80 m, and 5V:1H side slopes (Figure 2a). These  
150 proportions are based on typical crest dimensions for the core of earthfill dams in eastern Canada  
151 (SEBJ 1987). Different filter materials were placed around the core for each test. As the objective of this  
152 project was to make a preliminary survey of erosion mechanisms during core overtopping, effective stress  
153 conditions of actual dams were not reproduced: effective stresses were lower in the experimental model  
154 than in actual dams. Moreover, overall hydraulic gradients in the filters were higher than those observed  
155 in actual dam configurations where the width of the top of the core is larger (SEBJ 1987).

156           A plastic sheet with 14-mm holes and a nylon mesh with 1-mm openings allowed water to flow  
157 into the soil from the upstream reservoir (Figure 2a). The latter included a series of overflow drains to  
158 allow the upstream hydraulic head to be changed during core overtopping. A 5-mm-wide downstream  
159 outlet slot permitted both water and eroded particles to be collected in a sedimentation column. The  
160 overflow drains of the upstream reservoir and the sedimentation column flowed into a water tank located  
161 underneath the basin (Figure 2b). The water tank also collected fine particles not intercepted by the  
162 sedimentation column. Seepage was driven by gravity. The system was open as water at the outlet was  
163 not reused.

164           Tap water was used for this study. Water temperature was recorded during each test but was not  
165 controlled. Water temperatures for Tests 3, 4 and 4a were respectively 22, 23 and 15°C. Because Tests 1  
166 and 2 were conducted during winter, the water temperatures were significantly lower (respectively 3 and  
167 6 °C). Because of the large volume of water involved with each test, the water was not deaired before  
168 entering the test set-up. Since unsaturated flow is acknowledged in real dams (Saint-Arnaud 1995), it does  
169 not appear unrealistic to use regular tap water in the test set-up.

170           Two high-resolution colour cameras with softbox lighting were mounted in front of the basin  
171 (Figure 2c). The first camera recorded one image per second of the whole test setup with an 8-mm

172 objective. The second camera recorded three images per second of the downstream part of the core/filter  
173 interface with a 16-mm objective. This region of interest was chosen because erosion was initiated at the  
174 downstream edge of the core in previous experiments (Wörman and Skoglund 1992; Javadi and Mahdi  
175 2014). To prevent scratches, a transparent plastic film was applied on the inside of the sidewall that was  
176 filmed. Hydraulic head and suction were also measured in the core using six open piezometers and three  
177 pressure transducers with porous stones. Hydraulic head values are not presented herein, but have been  
178 discussed at length in Dumberry (2017).

179

## 180 **Granular Materials and Procedure**

181 Tests were conducted by combining different filter materials with the same core composed of till  
182 from northern Quebec. Three types of gravel (G1, G2 and G3) and one well-graded sand (2C) were used  
183 as filters. The well graded sand was representative of materials that have been used as filters for some  
184 dams in northern Quebec (Figure 3). Filter criteria from Fell et al. (2015) were used for the purpose of  
185 this study (see Table 1). Based on these criteria, the minimal value of  $D_{15}$  for the filter, the diameter of  
186 filter particles corresponding to 15% passing by mass, is determined by both the  $d_{85}$ , the diameter of core  
187 particles corresponding to 85% passing by mass, and the fines content,  $A$ , of the core material. In  
188 accordance with Table 1, filters must have a  $D_{15} \leq 0.7$  mm to fulfill the filter criteria applicable to  
189 embankment dams with broadly graded cores. As shown in Table 2, the three uniform gravel materials  
190 did not fulfill the filter criterion, while the 2C material did. One material had a  $D_{15}$  value relatively close  
191 to the filter criteria, while the two others were coarser. Filters G1, G2 and G3 were washed to remove  
192 fines prior to tests. Table 3 presents the effective diameter,  $D_{10}$ , the coefficient of uniformity,  $C_u$ , the  
193 relative density of solids  $D_R$ , the minimum and maximum values of the void ratio,  $e$ , the minimum and  
194 maximum values of the dry density,  $\rho_d$ , and the optimum water content,  $w_{opt}$ , of the materials used in this  
195 study. These parameters were determined using applicable ASTM standards (i.e. ASTM 2007; ASTM  
196 2012; ASTM 2014a; ASTM 2014b). As shown on Figure 3, the minimum particle size for materials G3

197 and 2C was lower than the width of the outlet slot. To prevent piping of the filter material through the slot  
198 during these tests, a fine layer of material G2 was placed along the width of the outlet slot.

199 The behaviour of the core material may influence the dam performance. In northern Quebec, glacial till  
200 deposits are generally characterized by a low plasticity index, a low compressibility and a high shear  
201 strength (Boulton 1977). They are well or broadly graded materials, which can be susceptible to  
202 suffosion and segregation (Sherard et al. 1984; Milligan 2003). However, their potentially unstable  
203 behaviour tends to be rectified by a self-healing process, as the fine particle that are eroded upstream  
204 gradually fill the pore network downstream, thus limiting the progression of erosion (Fell and Fry 2007).  
205 Lafleur et al. (1999) demonstrated that glacial tills from northern Quebec should be stable with respect to  
206 suffosion for a fines content higher than 12 %, which is the case for the till core used in this study  
207 (Table 3).

208 Table 4 presents the compaction state of the materials for each test. In accordance with practice  
209 (e.g. SEBJ 1987), the water content for the till during compaction was fixed slightly above the optimum  
210 water content of the standard Proctor compaction test (i.e.  $w_{opt} + 0.5$ ). The till was compacted in two  
211 12.5-cm thick layers. The core was compacted using a pneumatic hammer with a 5.1-cm square metal  
212 plate. A relative compaction, RC, of 97 % with respect to the maximal dry density from the standard  
213 Proctor compaction test was targeted. Filter materials that did not fulfill the filter criteria (Filters G1, G2  
214 and G3) were dumped to limit the impact of filter compaction on erosion. A relative density index,  $I_d$ , of  
215 70 % was aimed for material 2C. All materials were carefully placed to prevent segregation.

216 During each test, the water level was initially set 5 cm below the top of the core for a saturation  
217 period of 24 hours (first overflow level on Figure 2a). The duration of the saturation phase is critical since  
218 steady state conditions are more representative of actual field conditions. Numerical simulations using  
219 COMSOL presented in Dumberry et al. (2015) helped to predict the unsaturated behaviour of the tested  
220 specimens and to estimate the saturation period required for each increment. After the saturation period,

221 the water level was gradually increased by increments of 5 cm and held constant for 12 hours after each  
222 increment. The procedure was repeated until the maximum upstream water level was reached (eighth  
223 overflow level on Figure 2a). Depending on the filter material permeability, the maximum upstream water  
224 level was limited either by the maximum inlet flow rate (maximum flow rate of the faucet) or the  
225 elevation of the eighth overflow valve (Figure 2a). Test 3a was conducted at the end of Test 3 using the  
226 same specimen. For this test, the upstream water level was varied between its two extreme positions (i.e.  
227 levels 1 and 8) cyclically in time. For each cycle, the water level was held constant for 1 hour. Six cycles  
228 were completed for this test.

229         The model and the test procedures were designed to measure or calculate the parameters that  
230 affect the erosion mechanisms at the crest of an embankment dam. Pore pressures and suctions were  
231 recorded manually every 30 minutes with the open piezometers and automatically every 15 seconds with  
232 the pressure transducers. Flow rate and turbidity measurements were also obtained manually every  
233 30 minutes. Eroded sediments were collected at the outlet of the test setup to be weighted after drying and  
234 analyzed using sieve analysis for the sand fraction and laser diffraction for the fine fraction. At the end of  
235 each test, images recorded from the downstream camera were analyzed using DIC, while the images  
236 obtained from the general view mainly served to describe qualitatively the progression of erosion. For  
237 Tests 3 and 4,  $\mu$ CT analyses were completed on specimens collected using thin-walled aluminum  
238 samplers with a diameter of 10 cm and a length of 20 cm. The specimens were collected at the  
239 downstream and upstream edges of the top of the core, at the centre of the basin along the axis  
240 perpendicular to water flow (Figure 5e). Dumberry (2017) provides details on the specifications and  
241 parameters of the laser diffraction device, digital cameras, pressure transducers and the flowmeter. It also  
242 presents the turbidity and pore pressure results obtained during the tests. These results are not presented  
243 herein.

## **Digital Image Correlation and X-ray microcomputed tomography**

244 Digital image correlation (DIC), allows displacement and strain fields in a soil section to be computed  
245 (e.g. White et al. 2003). The principles of DIC can be summarized as follows. Several images are  
246 captured with a digital camera. Sub-images of image A (test patches) are compared with larger sub-  
247 images of image B (search patches). The most probable test patch displacement from image A within the  
248 search patches of image B is then estimated with a cross-correlation technique. This procedure is then  
249 repeated by comparing subsequent images, until all images have been examined. Displacement fields are  
250 computed from the conversion between pixel and length coordinates.  
251

252 For this project, images were analyzed using PIVlab (Thielicke and Stamhuis 2014a), an open-  
253 source MATLAB code for DIC. The displacements were calculated using a direct Fourier transform  
254 correlation with multiple passes (FFT window deformation). Pre-processing parameters included a filter  
255 enhancing the contrast in the images and two passes with interrogation areas varying from 512 to 256  
256 pixels. A calibration grid was placed on the wall prior to each test for pixel/length conversion. Aberrant  
257 vectors obtained during the analyses were removed with a standard deviation filter.

258 Microcomputed tomography is a non-destructive technique that uses the attenuation of X-rays to  
259 build a 3D reconstruction of a specimen. During a scan, a source sends X-rays that travel in straight lines  
260 through the specimen. Some of the X-rays are absorbed by the specimen, reducing their intensity. During  
261 the scan, the specimen is rotated about a vertical axis. For each position, X-ray attenuation forms a  
262 shadow image on a flat panel detector that converts the X-ray energy into light. After a full rotation of the  
263 specimen, its volume is divided into a large number of 3D cells (voxels). Using the shadow images, a  
264 linear X-ray attenuation value is estimated for each cell to create the 3D reconstitution of the object.  
265 Typically, voxels that display a strong X-ray attenuation (i.e. solid grains) are represented as brighter  
266 region, while darker regions represent materials with low attenuation (i.e. water and air in the voids).

267 For the purpose of this study, a XT H 225  $\mu$ CT scan from Nikon was used. For the scans  
268 presented in this paper, beam energy and current were respectively set to 221 kV and 184  $\mu$ A. The  
269 exposure time was set to 500 ms for each shadow image. The specimen location inside the  $\mu$ CT scan  
270 allowed a minimum voxel size of 80  $\mu$ m. As a result, it was not possible to distinguish individual fine  
271 particles in the till. A beam hardening correction was applied to the images to reduce streak artefacts from  
272 dense structures in the specimen. Beam hardening was also reduced using a copper filter placed between  
273 the X-ray source and the specimen. Preliminary segmentation and volume rendering were realized with  
274 Visual Graphics Studio MAX 2.2. Details on the parameters used for DIC and  $\mu$ CT analyses are presented  
275 in Dumberry (2017).

276

## 277 **Results**

### 278 **General observations**

279 Cameras allowed qualitative observation of erosion to be made for each test. Figure 4 shows  
280 photographs representing the state of the core/filter interface at 1) the initial stage of the test (before  
281 saturation), 2) when the water level is at the top of the core, and 3) at the end of the test. Results from  
282 Tests 1 and 2 showed significant erosion. For these core/filter combinations, erosion was first initiated  
283 locally along the downstream slope of the core, and then gradually progressed toward the horizontal  
284 interface as the upstream water level and hydraulic gradient increased, thus inducing a piping  
285 phenomenon (Fell and Fry 2007). As erosion progressed, the core material located above the pipe was  
286 continuously being eroded. Vertical settlements and reorganization of grains inside the filter material  
287 were also observed during the progression of the erosion. Tests 1 and 2 had to be stopped after reaching,  
288 respectively, the third and fourth upstream water levels because the flow rate at the inlet did not match the  
289 high permeability of the filter materials. Maximum flow rates of 45 and 41 L/min were measured for  
290 Tests 1 and 2, respectively, which correspond to water levels 3 and 4. At the end of these tests, particle re-

291 gradation was observed along the downstream slope (i.e. paving effect). As water velocities increased,  
292 fine particles were eroded preferentially at the downstream edge of the core. This allowed the remaining  
293 larger grains to act as a natural intermediate filter layer between the original filter and core materials.  
294 Figure 5a represents a detailed view of the core/filter downstream interface where a paving effect was  
295 observed.

296 Even though the filter material of Test 3 did not satisfy the filter criterion of Table 2, no  
297 significant erosion occurred. Some local instability appeared on the downstream slope (Figure 4), but no  
298 piping was observed within the core material. For Test 4, the filter material satisfied the filter criteria and  
299 no erosion occurred on the downstream slope or along the horizontal interface. Maximum flow rates of  
300 38 and 0.70 L/min were obtained for Tests 3 and 4, respectively, corresponding to water levels 8 and 7.

301 For all tests, local instabilities were observed during the saturation phase along the upstream slope  
302 of the core material. Erosion along the horizontal interface occurred mainly for Tests 1, 2 and 3, but was  
303 smaller in scale compared to the erosion observed along the downstream slope. For all water levels during  
304 which eroded particles were collected at the outlet, the propagation of erosion varied with time. For a 12-  
305 hour water level stage, erosion lasted less than 1 hour. Erosion apparently ceased after this initial erosion  
306 period, irrespective of the filter used here.

307

### 308 **Particle Size Distribution and Mass Balance**

309 Particle size distribution and mass balance analyses provided information on the propagation of  
310 erosion with time and the type of material being eroded. Table 5 presents mass balance results for each  
311 test. The percentage of eroded dry mass was computed considering the initial dry mass of the core  
312 material after placement (190.5 kg). Table 5 shows that major erosion was triggered when the upstream  
313 water level reached the core/filter interface (level 2) for Test 2. The same phenomenon was observed for  
314 Test 1, based on visual observation. For Test 3, erosion was initiated during level 3, when the water table

315 overtopped the core by 5 cm. However, no significant erosion occurred when the upstream water level  
316 was at the same elevation as the core/filter horizontal interface. For Tests 1 to 3, the greatest amount of  
317 eroded mass was collected during level 3. For Test 3a, the erosion rate gradually decreased as the number  
318 of cycles increased. These results suggest that, in some conditions, even a filter that does not meet filter  
319 criteria can control core particle erosion.

320 Figure 6 shows the particle-size distribution of the sediments eroded and collected at the outlet for  
321 each water level. The particle-size analyses demonstrate that the eroded particles tended to become  
322 coarser as the water level increased, especially for Tests 1 and 2. Eroded particles collected from levels 4  
323 to 8 for Test 3 were similar in terms of particle-size distributions. Particle-size gradation curves of  
324 sediments collected during Test 3a were finer than those obtained for levels 4 to 8 for Test 3.

325

### 326 **Digital Image Correlation**

327 Results for DIC are presented in Figure 7. Three images are shown for each test: the initial and  
328 the final stages as well as the computed displacement field. For Tests 1 and 2, a total of 63 and 34  
329 photographs were respectively used for the calculations. Displacement vectors are displayed at their real  
330 scale, which means that a vector length of 1 pixel represents a displacement of 1 pixel during the test. The  
331 DIC results show the complex distribution of displacement vectors (i.e. rapid orientation changes) where  
332 the pipe was formed. These rapid orientation changes are due both to large local deformations and patch  
333 comparison issues. The displacement vectors also show mean vertical settlements of approximately 7 and  
334 5 mm, for Tests 1 and 2, respectively, within the filter material at the downstream edge of the core  
335 material. The width of this settlement zone corresponds to the length of the erosion pipe. The settlement  
336 occurred simultaneously as the pipe progressed upward and as the core particles were eroded. In some  
337 parts of the section, for example over the edge of the core, the vertical displacements seem to increase  
338 downward, possibly indicating arching and an increase in porosity above the erosion zone. No major

339 particle displacements were observed within the core material, away from the interface and the pipe  
340 formation.

341 For Test 3, a total of 55 photographs were used for the calculations. Displacement vectors are  
342 represented at a magnified scale of 10:1 with a length of 10 pixels representing a displacement of 1 pixel.  
343 This magnification was used because particles displacements and the associated deformations were very  
344 small for this test relative to Tests 1 and 2. It can be noted that the displacements are concentrated at the  
345 downstream edge of the core. The mean vertical settlement is approximately 0.6 mm. No major migration  
346 of filter grains or contact erosion was observed. Results show that the vertical component of the  
347 displacement vector is predominant.

348 For Test 4, a total of 11 photographs were used for the calculations. Displacement vectors are  
349 represented with a scale of 75:1 as displacements were very small. The images show vertical  
350 settlements in the filter, and along the interface between till and filter, both at the top of the core and  
351 on the downstream slope. The mean vertical settlement within the filter is approximately 0.2 mm.  
352 Unlike Tests 1 and 2, local instabilities and vertical settlements due to erosion for Tests 3 and 4 are  
353 difficult to distinguish by simply comparing visually the initial and final photographs. The field of  
354 displacement vectors obtained in Test 4, where no erosion occurred, appears typical of the expected  
355 behaviour of a till core showing settlements during the wetting stage, therefore giving confidence to  
356 the DIC methods used herein.

357 The DIC results clearly show that the magnitude of the displacement vectors is related to the  
358 volume of till eroded during each test. Figure 8 shows the relationship between the mean displacement  
359 magnitude (in mm) obtained with DIC and the total eroded mass as a percentage of initial core mass as  
360 presented in Table 5. Results are presented for the complete tests and individual water level stages.  
361 The mass of fine sediments collected for each test in the water tank at the outlet of the sedimentation  
362 column was uniformly distributed among each water level. This assumption is a simplification as the

363 particle size distribution of the eroded sediments and the fraction of sediments that bypassed the  
364 sedimentation column varied with time. The mean displacement vector is subvertical for all tests,  
365 except for Test 4 that showed relatively small displacements. This is consistent with the displacement  
366 vectors presented in Figure 7. It should be noted that some of the eroded mass for Test 3 could come  
367 from the filter as 29 % of the G3 grain size distribution was finer than the slot width (5 mm).  
368 However, since there was no erosion for material 2C, it appears unlikely that material G3 was eroded  
369 through the slot.

370

### 371 **X-ray Microcomputed Tomography**

372 Figure 9 presents the  $\mu$ CT scan results for Tests 3 and 4 from different viewpoints. For Test 3, the  
373 scan shows local instabilities along the upstream slope during the saturation phase. The post-experiment  
374 downstream interface of the core is uneven and rougher than the initially undisturbed interface. This could  
375 be caused either by the hydraulic forces that eroded the core particles during the experiments, the effect of  
376 the compaction effort on the core surfaces regularity or the remoulding effects during sampling. For  
377 Test 4, a similar pattern was observed regarding local instabilities along the interfaces of the core/filter  
378 materials, with the exception that the irregularity seems to be less prominent. This is expected since no  
379 eroded particles were collected at the outlet of the test setup. Accordingly, the downstream plan view of  
380 the tested sample shows a relatively intact post-experiment core interface.

381

### 382 **Discussion**

383 Based on the results presented in Table 5, some particles from the core were collected at the test  
384 setup outlet for Tests 1 to 3. This implies that the three filters that did not meet the filter criteria did not  
385 contain pore constrictions that were small enough to retain the fine particles of the core material.  
386 However, for Test 3, even if the filter criteria were not fulfilled, only 0.25 % of the total dry mass of the  
387 till was eroded during the test, including the cyclic core overtopping stages at the end of the test. It is not

388 clear if this mass loss is significant. For comparison purposes, it has been observed that the global  
389 performance of the WAC Bennett Dam, located in British Columbia, Canada, was affected by a much  
390 smaller percentage of mass loss (Garner and Fannin 2010). Indeed, the presence of two sinkholes of at  
391 least 1,400 m<sup>3</sup> within a total volume of about 2.5×10<sup>7</sup> m<sup>3</sup> of till material caused significant changes in  
392 flow rates and pressure measurements within the dam. Based on this comparison, it can be inferred that  
393 erosion rates as low as 0.25 % could potentially have a negative influence on the performances of  
394 embankment dams. It thus appears important to put more effort on the modelling, both numerical and  
395 physical, of the evolution of minor erosion events for embankment dams. Better modelling tools would  
396 allow erosion thresholds to be defined.

397 Visual analysis of erosion was useful to understand the erosion mechanisms at the top of the core.  
398 For Tests 1 and 2, piping was initiated along the downstream slope, before complete core overtopping  
399 (Figure 4). Erosion along the downstream slope of the core during overtopping experiments has been  
400 observed by other researchers (e.g. Gregoretti et al. 2010; Javadi and Mahdi 2014). However, in these  
401 cases, piping developed while the core material was completely saturated and overtopped. A review of the  
402 photographs for Tests 1 and 2 shows the pipe to be parallel to the streamline delimiting the  
403 saturated/unsaturated conditions within the core. For Tests 1 and 2, it appears that contact erosion at the  
404 horizontal interface between till and filter was less significant than the erosion due to piping. Based on  
405 these results, it can be inferred that erosion of the downstream slope would be more critical than erosion  
406 along the core/filter horizontal interface for actual dams. Also, hydraulic gradients before core  
407 overtopping would be much higher for a real dam. As a result, piping along the downstream slope of the  
408 core would probably be initiated before the water level reached the top of the core. This implies that  
409 combinations of filter and core materials that are stable when the water level is below the core summit  
410 would not be negatively impacted by core overtopping.

411 A qualitative examination of the post-experiment results from Tests 1 and 2 reveals the  
412 development of graded bedding along the downstream slope (Figure 5a). Three different materials were

413 identified. As fine particles from the till were eroded through the filter, the core material along the  
414 downstream interface became coarser. This created a relatively uniform intermediate filter layer that was  
415 coarser than the original core material, but finer than the filter. This phenomenon, known as paving or  
416 bridging, has been observed previously for broadly graded core materials (e.g. Lafleur et al. 1989;  
417 Wörman 1996; Dionne and Konrad 2015). Other researchers have referred to the self-healing capability  
418 of broadly graded materials (e.g. Milligan 2003; Fell and Fry 2007). A post-test visual analysis of the  
419 surfaces of the core material for Test 2 showed a much coarser matrix at the downstream edge of the core  
420 (Figure 5d) compared to the upstream edge (Figure 5c). As shown on Figure 5d, erosion was relatively  
421 homogeneous along the width of the test setup.

422         According to Table 5, the percentage of eroded particles decreased with time after a critical water  
423 level was reached. Therefore, as observed by Wörman and Olafsdottir (1992), the erosion rate did not  
424 correlate with the upstream water level once the erosion was initiated. Wörman and Olafsdottir (1992)  
425 explained this trend in terms of hydraulic gradient. The paving effect described previously probably also  
426 explains why the erosion rate decreased during the later stages of each test.

427         Approximate water velocity values in the filter above the erosion surface can be calculated from  
428 the flow rate at the outlet and the saturated thickness of the filter material (Figure 4, end of final stage).  
429 Seepage velocity values of 3.9 and 2.1 cm/s are calculated respectively for Tests 1 and 2. Real pore water  
430 velocity values of 10.5 and 5.8 cm/s can be obtained for the same tests by dividing the seepage velocity  
431 values by the G1 and G2 filter porosity values ( $e/(e+1)$  in Table 4). These water velocity values are  
432 relatively close to the critical velocity of 10 cm/s for interfacial erosion and bridge scour for non-plastic  
433 fines and fine sand (Briaud 2008), and very high with respect to the critical velocity for piping (Richards  
434 and Reddy 2012). This could explain the prevalence of piping failure and the paving effect which would  
435 correspond to the erosion of fine sand and non-plastic fines (Figure 6).

436 For Test 4, the correctly designed filter material was efficient at retaining the core particles. No  
437 particles were collected at the test setup outlet. Important differences between the test setup and actual  
438 field conditions must however be noted. First, the filter material used for this test was densely compacted.  
439 However, for actual field conditions, under-compacted zones are likely to be found in areas where  
440 material placement poses challenges, for instance in the vicinity of instruments or spillways. In that sense,  
441 some studies have demonstrated that filter criteria should be revised for under-compacted core material  
442 (Watabe et al. 2000; Soroush et al. 2016).

443 The degree of segregation and heterogeneity is also a significant difference between the  
444 laboratory model presented in this paper and actual field conditions. Milligan (2003) mentioned that  
445 internal erosion of broadly graded till is more likely to be the consequence of segregation during  
446 placement rather than from hydraulic conditions or geometric instability. For this laboratory study,  
447 placement of filter G3 created thin layers of coarser material and discontinuous voids within the filter  
448 (Figure 5b). These coarse-grained layers influenced the path followed by the eroded core particles, as they  
449 tended to migrate horizontally within these layers. Segregation of filter 2C for Test 4 also created  
450 localized void networks along the upstream interface. Local instabilities were observed in these large  
451 voids (Figure 4). Wörman and Olafsdottir (1992) and Smith (2012) also acknowledged that even limited  
452 spatial variations in soil characteristics can increase the risk of erosion.

453 DIC provided interesting results regarding contact erosion between two granular materials. This  
454 technique was able to calculate the displacements in the material surrounding the erosion zones. However,  
455 the high local deformation rates associated with particles migration or seepage were not always handled  
456 properly by this technique. For instance, Figure 7 showed the presence of randomly oriented vectors  
457 along the pipe. Changes in water content and the fine texture of the till with respect to the resolution of  
458 the photographs are other issues with DIC for this model. DIC remains a promising tool for studying  
459 erosion processes despite these limitations. PIV algorithms that handle discrete displacement have

460 recently been developed (e.g. Andò et al. 2012). These algorithms could help modify PIVlab to consider  
461 erosion.

462 Reconstruction of  $\mu$ CT models provided additional information on erosion away from the  
463 sidewalls of the test setup. Along with DIC analyses and photographs of the post-test core material  
464 (Figures 5c and 6d),  $\mu$ CT demonstrates that the influence of sidewall on erosion was negligible.  
465 Reconstruction of  $\mu$ CT models remains a relatively new tool in geotechnical engineering. With proper  
466 segmentation techniques (e.g. Taina et al. 2007; Kim et al. 2013), the local grain size distribution of the  
467 intermediate filter associated with paving could be calculated.  $\mu$ CT analyses can also give detailed  
468 morphological information about the shape, size distribution and connectivity of the pore network within  
469 the specimen. This could provide interesting information knowing that some researchers recently studied  
470 the effect of constriction size in soils on their geotechnical behaviour (Indraratna et al. 2011; Shire et al.  
471 2014; To et al. 2015).

472

## 473 **Conclusion**

474 In Quebec, most large dams are zoned earthfill structures with a glacial till core protected by  
475 filters. This paper looked at the erosion mechanisms at the local scale during core overtopping by using a  
476 physical model representative of most field conditions, and image processing techniques such as DIC and  
477  $\mu$ CT. In total, four tests involving impoundment of the upstream reservoir eventually above the core top  
478 were performed with the same core material, a glacial till from northern Quebec, and different filter  
479 materials. The first three tests were conducted with uniform gravel filters with  $D_{15}$  of 22 mm (G1), 8 mm  
480 (G2) and 2.5 mm (G3). These filters did not fulfill the filter criteria considered. The fourth filter, a well-  
481 graded sand with a  $D_{15}$  of 0.5 mm (2C), satisfied the filter criteria and was more representative of actual  
482 field conditions. Hydraulic boundaries were defined by a variable upstream water level initially fixed  
483 5 cm under the top of the core for a saturation phase of 24 hours. Water levels were then increased by

484 increments of 5 cm each 12 hours. Combination of the till core and filter G3 was also tested by varying  
485 cyclically the water level from the highest to the lowest levels.

486 No eroded particles were collected downstream for the test involving filter 2C. Uniform gravel  
487 filters did not adequately protect the core material, since eroded particles were collected downstream. The  
488 most pronounced erosion was associated with the coarsest filter material. For the tests involving Filters  
489 G1 and G2, a pipe appeared along the downstream slope when the water level reached the top of the core.  
490 The pipe was parallel to the flow line. Erosion during these tests was mainly due to the progression of the  
491 pipe within the core material rather than contact erosion along the horizontal interface. For the first three  
492 tests, erosion mainly occurred when the water level reached the core/filter interface and the subsequent  
493 level. The erosion rate decayed in time as the hydraulic gradient increased. The self-healing process that  
494 was observed at the interface between core and filter explains this decrease in erosion rate. For each water  
495 level increment, erosion mainly took place during the first hour of the imposed hydraulic condition.

496 The DIC technique clearly showed that the displacement vector magnitude is directly proportional  
497 to the volume of till eroded. DIC results provided detailed information on the vertical settlements and  
498 grains reorganization within the filter material, as the core was being eroded.  $\mu$ CT results put the  
499 emphasis on the post-experiment downstream interface of the core, which became uneven and rougher  
500 than the initially undisturbed interface as the hydraulic gradient increased. For filters G3 and 2C, results  
501 showed that erosion mainly appeared along the downstream slope.  $\mu$ CT also showed that there was no  
502 wall effect with the setup and conditions used herein.

503 Experimental results for this study will further be analyzed using a numerical model based on a  
504 multiscale approach, combining particle scale modelling with the discrete element method (open-source  
505 code YADE), and COMSOL. Upcoming experimental runs will also be conducted using the same setup  
506 to study the effect of unsaturated conditions in embankment dams on internal erosion. The reduced-scale  
507 nature of this study nevertheless necessitates caution with regards to the inferences drawn for large

508 embankment dams. The effect of the spatial configuration of the soil components must also be  
509 considered. Further experimental studies should focus on the downstream slope stability of the core  
510 material in core overtopping conditions. Filter efficiency in such conditions is also an issue, as to whether  
511 pore pressures, flow rates and effective stress have an impact on the filter performance.

512

## 513 **Acknowledgments**

514 The authors are grateful to the Natural Sciences and Engineering Research Council of Canada  
515 (NSERC) and Hydro-Québec for their financial support through a Collaborative Research and  
516 Development grant (CRD). The authors would like to acknowledge the technical support of Sébastien  
517 Ménard for the design and construction of the test setup and the help of two graduate students who  
518 monitored the test setup at night. The authors would also like to thank two anonymous reviewers whose  
519 comments and suggestions helped to improve the manuscript.

520

## 521 **References**

- 522 Andò, E., Hall, S.A. and Viggiani, G. 2012. Grain-scale experimental investigation of localised  
523 deformation in sand: a discrete particle tracking approach. *Acta Geotechnica*, 7: 1-13.
- 524 ASTM. 2007. Standard test method for particle-size analysis of soils (D 422). ASTM International, West  
525 Conshohocken, PA, USA.
- 526 ASTM. 2012. Standard test methods for laboratory compaction characteristics of soil using standard  
527 effort (12 400 ft-lbf<sup>3</sup> (600 kN-m/m<sup>3</sup>)) (D 698). ASTM International, West Conshohocken, PA,  
528 USA.
- 529 ASTM. 2014a. Standard test methods for maximum index density and unit weight of soils using a  
530 vibratory table (D 4253). ASTM International, West Conshohocken, PA, USA.

- 531 ASTM. 2014b. Standard test methods for minimum index density and unit weight of soils and calculation  
532 of relative density (D 4254). ASTM International, West Conshohocken, PA, USA.
- 533 Beguin, R., Philippe, P. and Faure, Y.H. 2013. Pore-scale flow measurements at the interface between a  
534 sandy layer and a model porous medium: application to statistical modeling of contact erosion.  
535 *Journal of Hydraulic Engineering*, **139**(1): 1-11.
- 536 Binner, R., Homberg, U., Prohaska, S., Kalbe, U. and Witt, K.J. (2010). Identification of descriptive  
537 parameters of the soil pore structure using experiments and  $\mu$ CT data. *In Proceedings of the 5th*  
538 *International Conference on Scour and Erosion*, San Francisco, CA, USA, 7-10 November 2010.  
539 ASCE, Reston, VA, USA, pp. 397-407.
- 540 Boccalini, F., Chen, Z., Omidva, M. and Iskander, M. 2015. A study of plane strain pile jacking and  
541 driving in granular media. *In Proceedings of the International Foundations Congress and*  
542 *Equipment Expo (IFCEE)*, San Antonio, TX, USA, 17-21 March 2015. ASCE, Reston, VA, USA,  
543 pp. 738-747.
- 544 Boulton, G.W. 1977. The development of geotechnical properties in glacial tills. *In Glacial till: An inter-*  
545 *disciplinary study. Edited by R. F. Legget.* The Royal Society of Canada in co-operation with the  
546 National Research Council of Canada, Ottawa, ON, Canada. pp. 292-303.
- 547 Briaud, J.L. 2008. Case Histories in Soil and Rock Erosion: Woodrow Wilson Bridge, Brazos River  
548 Meander, Normandy Cliffs, and New Orleans Levees. *Journal of Geotechnical and*  
549 *Geoenvironmental Engineering*, **134**(10): 1425-1447.
- 550 Chapuis, R.P. 2004. Predicting the saturated hydraulic conductivity of sands and gravel using effective  
551 diameter and void ratio. *Canadian Geotechnical Journal*, **41**(5): 787-795.
- 552 Chapuis, R.P. 2012. Predicting the saturated hydraulic conductivity of soils: A review. *Bulletin of*  
553 *Engineering Geology and the Environment*, **71**(3): 401-434.
- 554 Dionne, P.O. and Konrad, J.M. 2015. An experimental study of contact erosion between a till core and  
555 coarser crest and filter material. *In Proceedings of the 68th Canadian Geotechnical Conference*

- 556 and 7th Canadian Permafrost Conference, Quebec city, QC, Canada, 20-23 September 2015.  
557 Canadian Geotechnical Society, Richmond, BC, Canada.
- 558 Dumberry, K. 2017. Étude expérimentale des mécanismes d'érosion durant le franchissement de noyau.  
559 Master Thesis, Department of Construction Engineering, École de technologie supérieure,  
560 Montréal, QC, CAN.
- 561 Dumberry, K., Duhaime, F. and Éthier, Y.A. 2015. Experimental study of contact erosion during core  
562 overtopping. *In* Proceedings of the Canadian Dam Association Annual Conference, Mississauga,  
563 ON, Canada, 3-8 October 2015. Canadian Dam Association, Toronto, ON, Canada, pp. 214-218.
- 564 Fell, R. and Fry, J.J. 2007. The state of the art of assessing the likelihood of internal erosion of  
565 embankment dams, water retaining structures and their foundations. *In* Internal erosion of dams  
566 and their foundations. *Edited by* R. Fell and J.J. Fry. Taylor & Francis, London, UK. pp. 1-23.
- 567 Fell, R., MacGregor, P., Stapledon, D., Bell, G. and Foster, M. 2015. Geotechnical engineering of dams.  
568 Taylor & Francis, London, UK.
- 569 FEMA. 2014. Technical manual: Overtopping protection for dams. Best practices for design,  
570 construction, problem identification and evaluation, inspection, maintenance, renovation and  
571 repair. FEMA P-1015, USBR, Denver, CO, USA.
- 572 Foster, M., Fell, R. and Spannagle, M. 2000. Statistics of embankment dam failures and accidents.  
573 Canadian Geotechnical Journal, **37**(5): 1000-1024.
- 574 Garner, S.J. and Fannin, R.F. 2010. Understanding internal erosion: A decade of research following a  
575 sinkhole event. *International Journal on Hydropower and Dams*, **17**(3): 93-98.
- 576 Gregoretti, C., Maltauro, A. and Lanzoni, S. 2010. Laboratory experiments on the failure of coarse  
577 homogeneous sediment natural dams on a sloping bed. *Journal of Hydraulic Engineering*,  
578 **136**(11): 868-879.
- 579 Guidoux, C., Faure, Y.H., Beguin, F. and Ho, C.C. 2010. Contact erosion at the interface between  
580 granular coarse soil and various base soils under tangential flow condition. *Journal of*  
581 *Geotechnical and Geoenvironmental Engineering*, **136**(5): 741-750.

- 582 Indraratna, B., Nguyen, V. and Rujikiatkamjorn, C. 2011. Assessing the potential of internal erosion and  
583 suffusion of granular soils. *Journal of Geotechnical and Geoenvironmental Engineering*, **137**(5):  
584 550-554.
- 585 Javadi, N. and Mahdi, T.F. 2014. Experimental investigation into rockfill dam failure initiation by  
586 overtopping. *Natural Hazards*, **74**: 623-637.
- 587 Kim, F.H., Penumadu, D., Gregor, J., Kardjilov, N. and Manke, I. 2013. High-resolution neutron and X-  
588 ray imaging of granular materials. *Journal of Geotechnical and Geoenvironmental Engineering*,  
589 **139**(5): 715-723.
- 590 Lafleur, J., Mlynarek, J. and Rollin, A.L. 1989. Filtration of broadly graded cohesionless soils. *Journal of*  
591 *Geotechnical Engineering*, **115**(12): 1747-1768.
- 592 Lafleur, J., Montès, P. and Alicescu, V. 1999. Internal stability of particles in dam cores made of broadly  
593 graded moraines. *In Proceedings of the 52nd Canadian Geotechnical Conference, Regina, SK,*  
594 *Canada, 25-27 October 1999. Canadian Geotechnical Society, Richmond, BC, Canada, pp. 551-*  
595 *558.*
- 596 Maknoon, M. and Mahdi, T.F. 2010. Experimental investigation into embankment external suffusion.  
597 *Natural Hazards*, **54**(3): 749-763.
- 598 Milligan, V. 2003. Some uncertainties in embankment dam engineering. *Journal of Geotechnical and*  
599 *Geoenvironmental Engineering*, **129**(9): 785-797.
- 600 Pan, B., Qian, K., Xie, H. and Asundi, A. 2009. Two-dimensional digital image correlation for in-plane  
601 displacement and strain measurement: A review. *Measurement, Science and Technology*, **20**: 1-  
602 17.
- 603 Pirnia, P., Duhaime, F., Éthier, Y.A., Dubé, J.S. 2016. Development of a multiscale numerical modelling  
604 tool for granular materials. *In Proceedings of the 69th Canadian Geotechnical Conference,*  
605 *Vancouver, BC, Canada, 2-5 October 2016. Canadian Geotechnical Society, Richmond, BC,*  
606 *Canada.*

- 607 Richards, K.S., and Reddy, K.R. 2012. Experimental investigation of initiation of backward piping in  
608 soils. *Géotechnique*, **62**(10): 933-942.
- 609 SEBJ. 1987. Le complexe hydroélectrique de La Grande Rivière : Réalisation de la première phase.  
610 Chenelière, Montreal, QC, Canada.
- 611 Saint-Arnaud, G. 1995. The high pore pressure within embankment dams: an unsaturated soil approach.  
612 *Canadian Geotechnical Journal*, **32**: 892-898.
- 613 Seo, M.W., Ha, I.S., Im, E.S., Kim, H.S., Kim, Y.S., and Kim, T.H. 2006. Centrifuge tests for evaluating  
614 effects of water level change on fill dam behavior. *In Proceedings of the 6th International*  
615 *Conference on Physical modelling in Geotechnics*, Honk Kong, 4-6 August 2006. Taylor &  
616 Francis, London, UK, pp. 431-434.
- 617 Sherard, J.L., Dunnigan, L.P. and Talbot, J.R. 1984. Basic properties of sand and gravel filters. *Journal of*  
618 *Geotechnical Engineering*, **110**(6): 684-700.
- 619 Shire, T., O'Sullivan, C., Hanley, K.J. and Fannin, R.J. 2014. Fabric and effective stress distribution in  
620 internally unstable soils. *Journal of Geotechnical and Geoenvironmental Engineering*, **140**(72): 1-  
621 11.
- 622 Smith, M. 2012. Assessment of the internal stability of a dam core. *La Houille Blanche*, (4-5): 54-59.
- 623 Soroush, A., Tabatabaie Shourijeh, P. and Shams Molavi, S. 2016. Applicability of filter design criteria  
624 for wet core embankment dams in wet climates. *Geotechnical Testing Journal*, **39**(3), 343-361.
- 625 Taina, I.A., Heck, R.J. and Elliot, T.R. 2007. Application of X-ray microcomputed tomography to soil  
626 science: A literature review. *Canadian Journal of Soil Science*, **88**(1): 1-19.
- 627 Takano, D., Lenoir, N., Otani, J. and Hall, S.A. 2015. Localised deformation in a wide-grained sand under  
628 triaxial compression revealed by X-ray tomography and digital image correlation. *Soils and*  
629 *Foundations*, **55**(4): 906-915.
- 630 Thielicke, W. and Stamhuis, E.J. 2014a. PIVlab (version 1.41).  
631 <http://dx.doi.org/10.6084/m9.figshare.1092508>.

- 632 Thielicke, W. and Stamhuis, E.J. 2014b. PIVlab – Towards user-friendly, affordable and accurate Digital  
633 Particle Image Velocimetry in MATLAB. *Journal of Open Research Software*, **2**:e30.
- 634 To, H.D., Galindo-Torres, S.A. and Scheuermann, A. 2015. Primary fabric fraction analysis of granular  
635 soils. *Acta Geotechnica*, **10**: 375-387.
- 636 Tollner, E.W. and Verma, B.P. 1989. X-Ray  $\mu$ CT for quantifying water content at points within a soil  
637 body. *Soil and Water Division of ASAE*, **32**(3): 901-905.
- 638 Van Beek, V.M., Van Essen, H.M., Vandenboer, K., Bezuijen, A. 2015. Developments in modelling of  
639 backward erosion piping. *Géotechnique*, **65**(9): 740-754.
- 640 Watabe, Y., Leroueil, S. and Le Bihan, J.P. 2000. Influence of compaction conditions on pore-size  
641 distribution and saturated hydraulic conductivity of a glacial till. *Canadian Geotechnical Journal*,  
642 **37**: 1184-1194.
- 643 White, D.J., Take, W.A. and Bolton, M.D. 2003. Soil deformation measurement using particle image  
644 velocimetry (PIV) and photogrammetry. *Géotechnique*, **55**(7): 619-631.
- 645 Wörman, A. 1996. Constitutive equation for filtration of well graded base soil with flow parallel to  
646 base/filter interface. *In Proceedings of 2nd International Conference on Geofilters*, Montreal, QC,  
647 Canada, May 1996. Bitech Publishers, Richmond, BC, Canada, pp. 295-304.
- 648 Wörman, A. and Olafsdottir, R. 1992. Erosion in a granular medium interface. *Journal of Hydraulic*  
649 *Research*, **30**(5): 639-655.
- 650 Wörman, A. and Skoglund, M. 1992. Overtopping of the core in rockfill dams - Internal erosion. *In*  
651 *Proceedings of the 2nd International Conference on Hydropower Development*, Lillehammer,  
652 Norway, 16-18 June 1992. A.A. Balkema, Rotterdam, Netherlands, pp. 433-440.
- 653 Zhang, L.M. and Chen, Q. 2006. Seepage failure mechanism of the Gouhou rockfill dam during reservoir  
654 water infiltration. *Soils and Foundations*, **46**(5): 557-568.
- 655
- 656

657 **Figure Captions**

658 Figure 1: Schematic representation of core overtopping

659 Figure 2: (a) Layout of the physical model; (b) Photograph of the front of the model; (c) Photograph of  
660 the back of the model

661 Figure 3: Particle-size distribution of the till core and filter materials

662 Figure 4: Photographs of Tests 1-4 before saturation, at the end of the stage during which the water level  
663 was maintained at the core/filter interface and at the end of each test

664 Figure 5: (a) Intermediate filter layer created by paving at the downstream edge of the core for Test 1  
665 (backside of the model); (b) Influence of segregation on migration patterns of eroded particles for Test 3  
666 (frontside of the model); (c) Horizontal and sloped surfaces at the upstream edge (top view) of the core  
667 for Test 2; (d) Horizontal and sloped surfaces at the downstream edge (top view) of the core for Test 2;  
668 (e)  $\mu$ CT sampling locations

669 Figure 6: Particle-size distribution of the eroded mass collected: (a) Tests 1-2; (b) Tests 3-3a

670 Figure 7: Results from DIC analyses of two recorded images during an erosion stage for Tests 1-4 (vector  
671 scales for each test are shown on the figure)

672 Figure 8: Relationship between mean displacement magnitude and total eroded mass as a percentage of  
673 initial core mass

674 Figure 9:  $\mu$ CT results of downstream and upstream samples for Tests 3 and 4 from different viewpoints

675

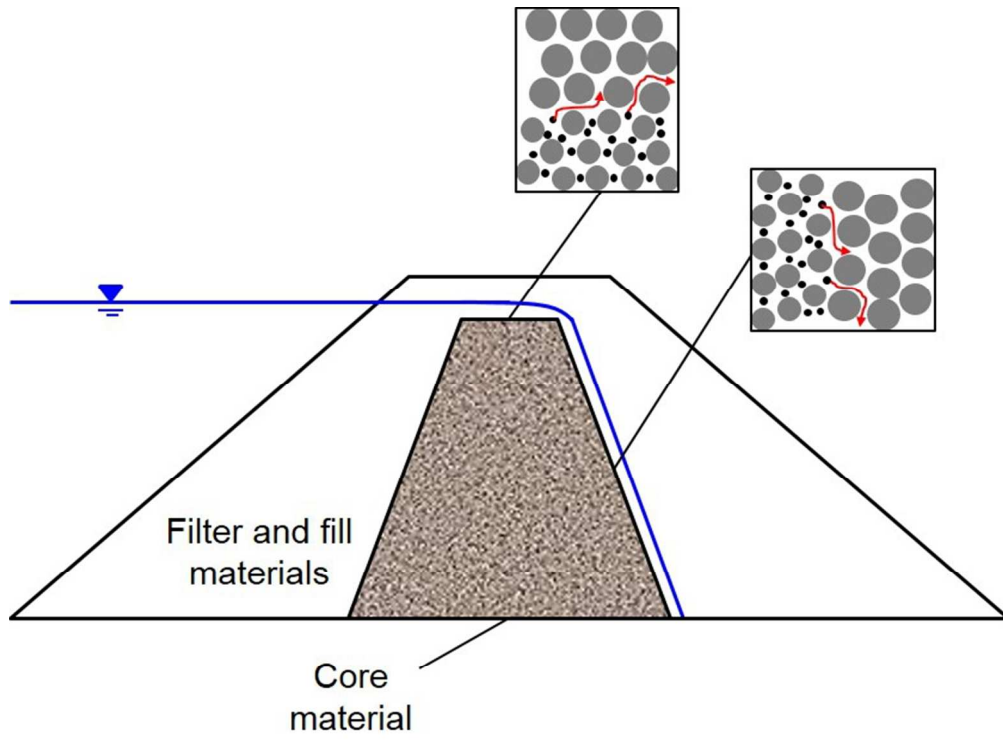


Figure 1: Schematic representation of core overtopping

142x107mm (150 x 150 DPI)

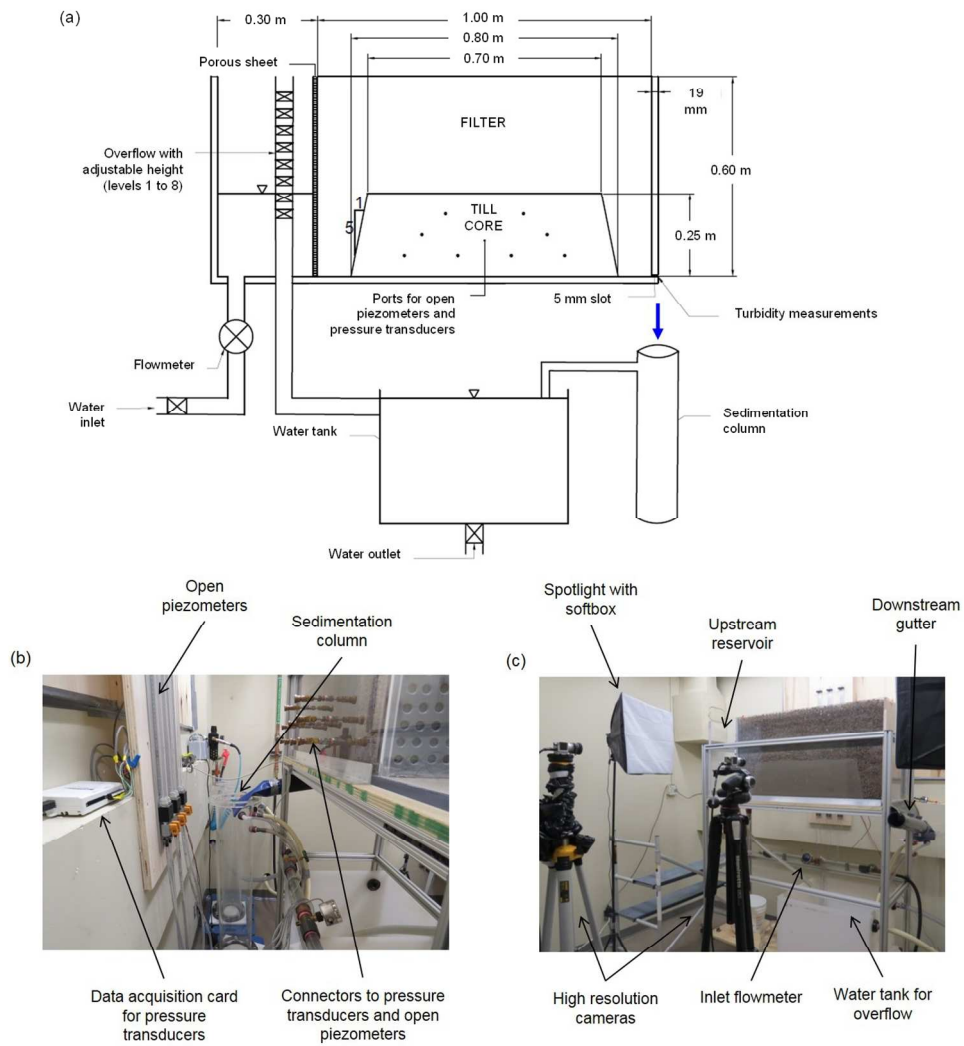


Figure 2: (a) Layout of the physical model; (b) Photograph of the front of the model; (c) Photograph of the back of the model

246x264mm (150 x 150 DPI)

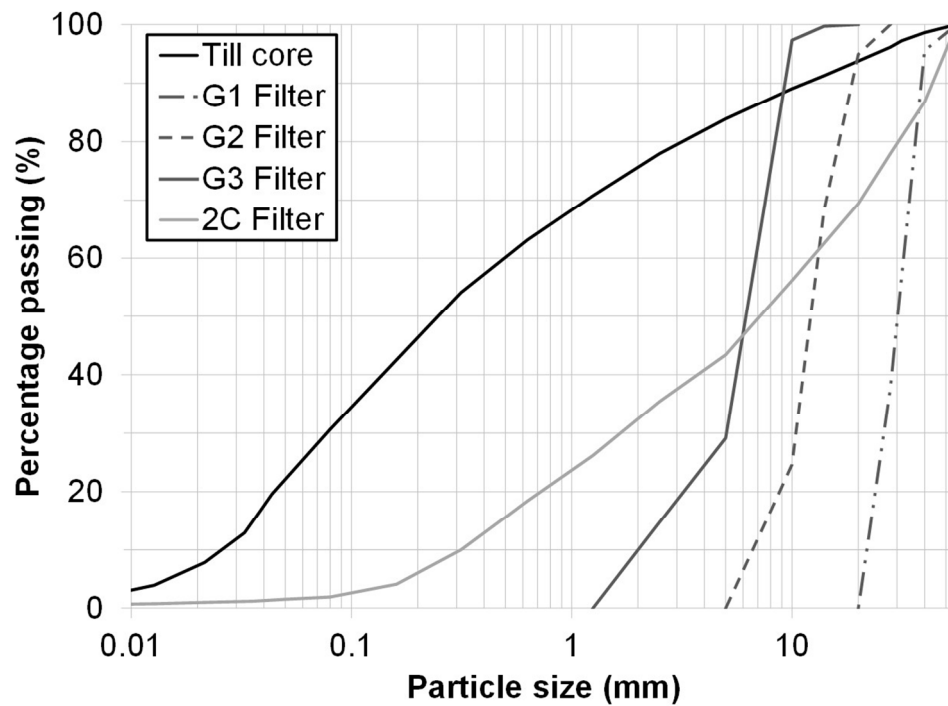


Figure 3: Particle-size distribution of the till core and filter materials

222x161mm (150 x 150 DPI)

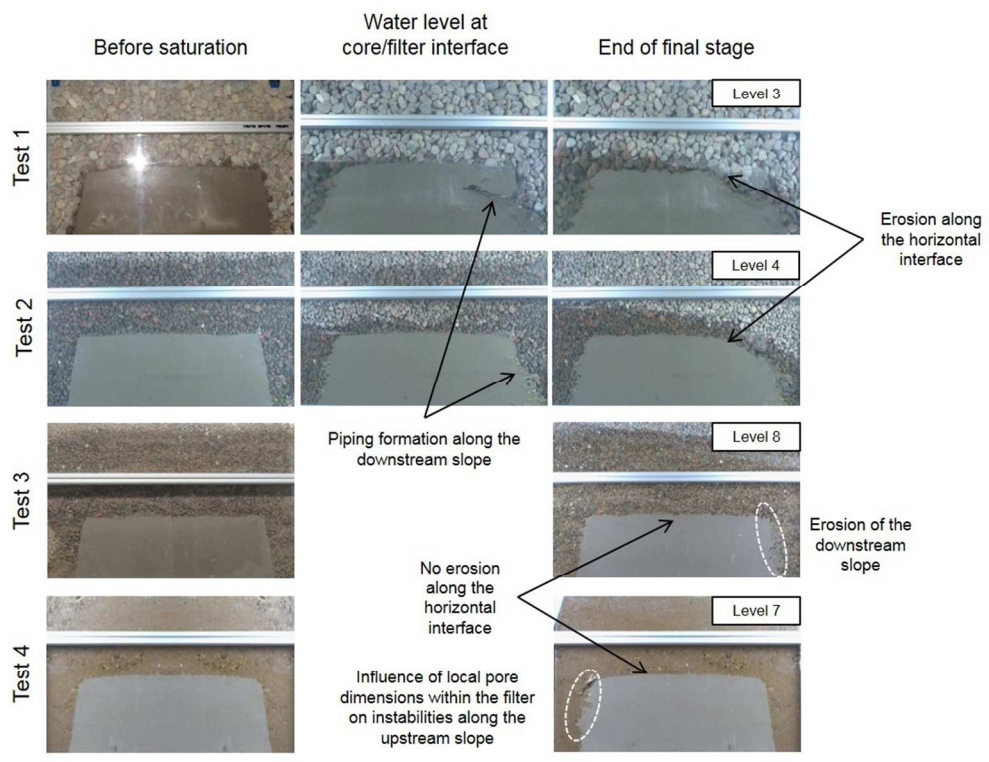


Figure 4: Photographs of Tests 1-4 before saturation, at the end of the stage during which the water level was maintained at the core/filter interface and at the end of each test

191x146mm (150 x 150 DPI)

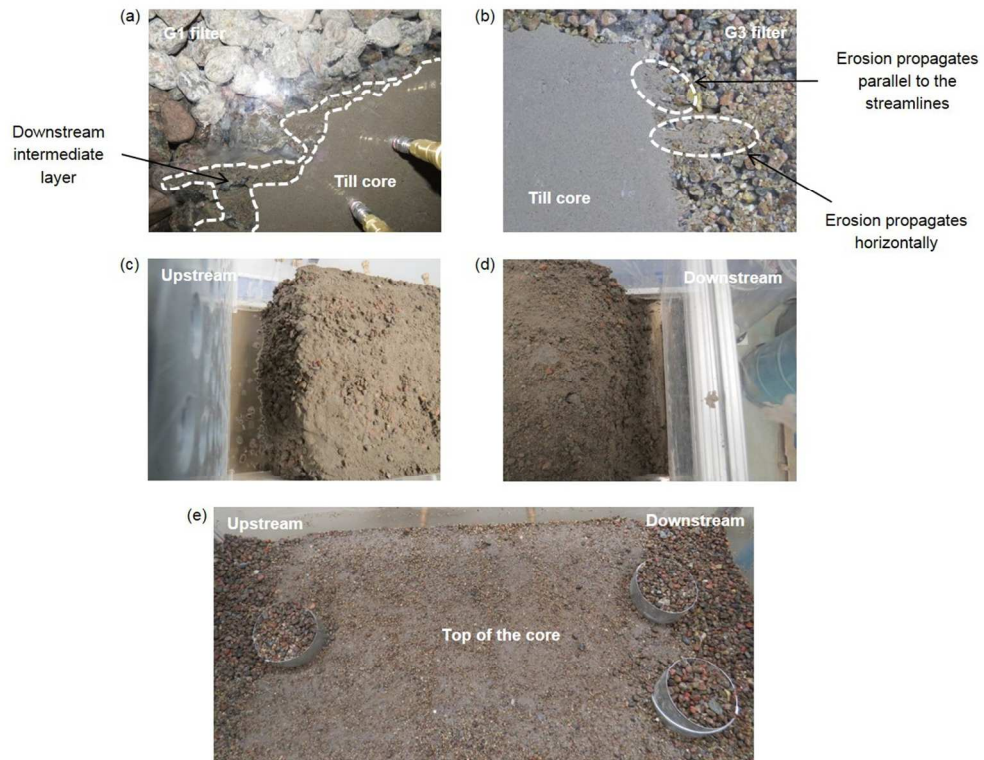


Figure 5: (a) Intermediate filter layer created by paving at the downstream edge of the core for Test 1 (backside of the model); (b) Influence of segregation on migration patterns of eroded particles for Test 3 (frontside of the model); (c) Horizontal and sloped surfaces at the upstream edge (top view) of the core for Test 2; (d) Horizontal and sloped surfaces at the downstream edge (top view) of the core for Test 2; (e)  $\mu$ CT sampling locations

213x162mm (150 x 150 DPI)

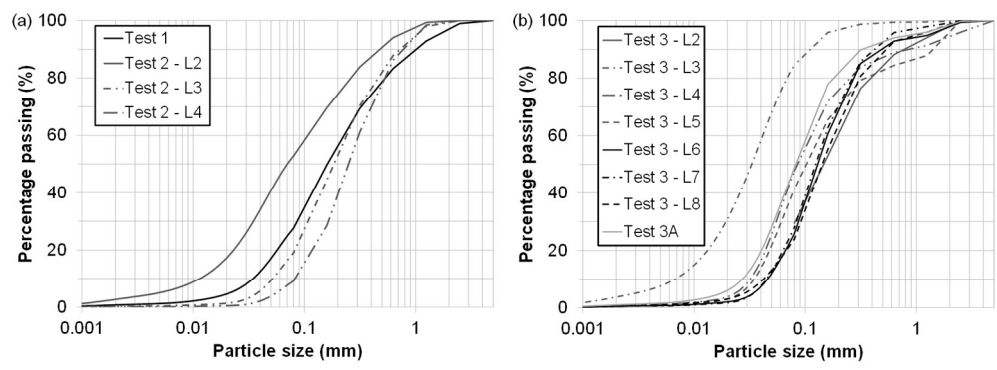


Figure 6: Particle-size distribution of the eroded mass collected: (a) Tests 1-2; (b) Tests 3-3a

284x103mm (150 x 150 DPI)

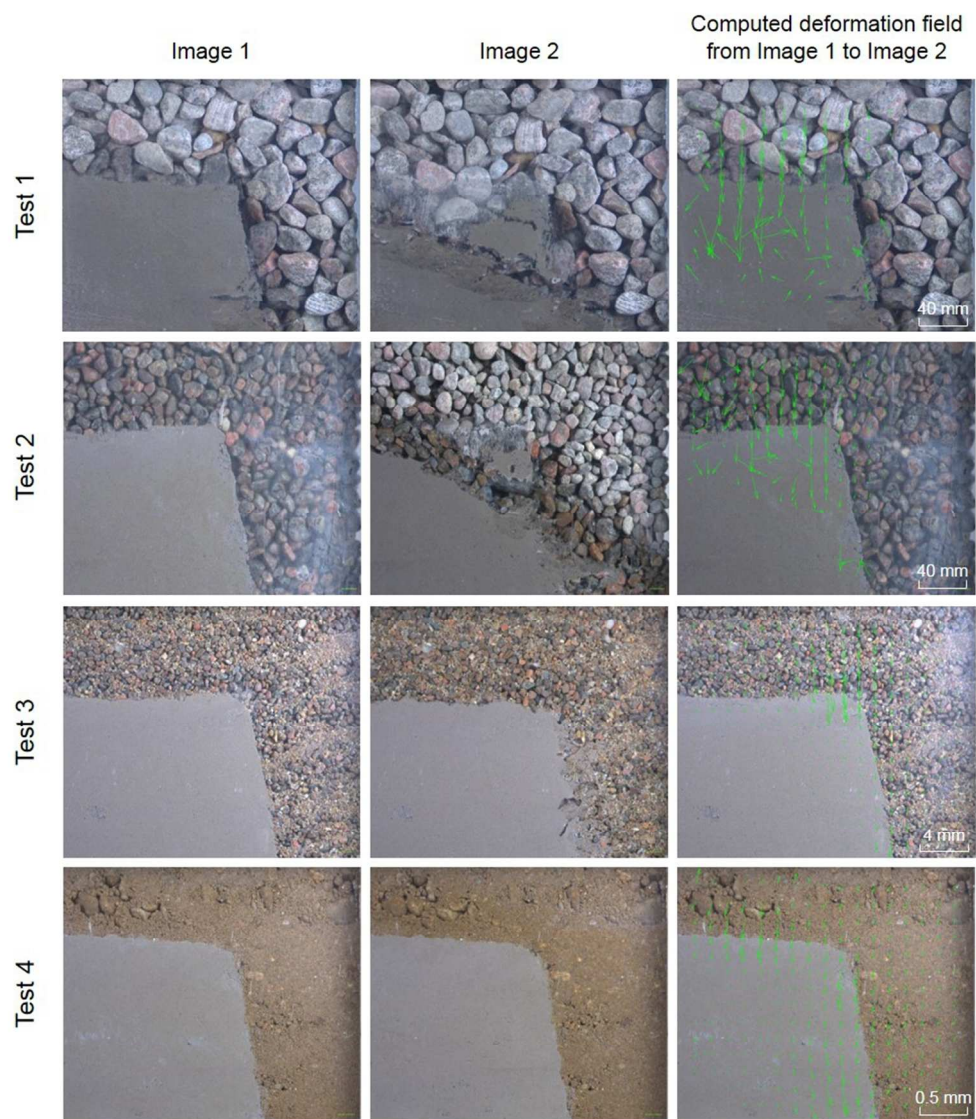


Figure 7: Results from DIC analyses of two recorded images during an erosion stage for Tests 1-4 (vector scales for each test are shown on the figure)

167x196mm (150 x 150 DPI)

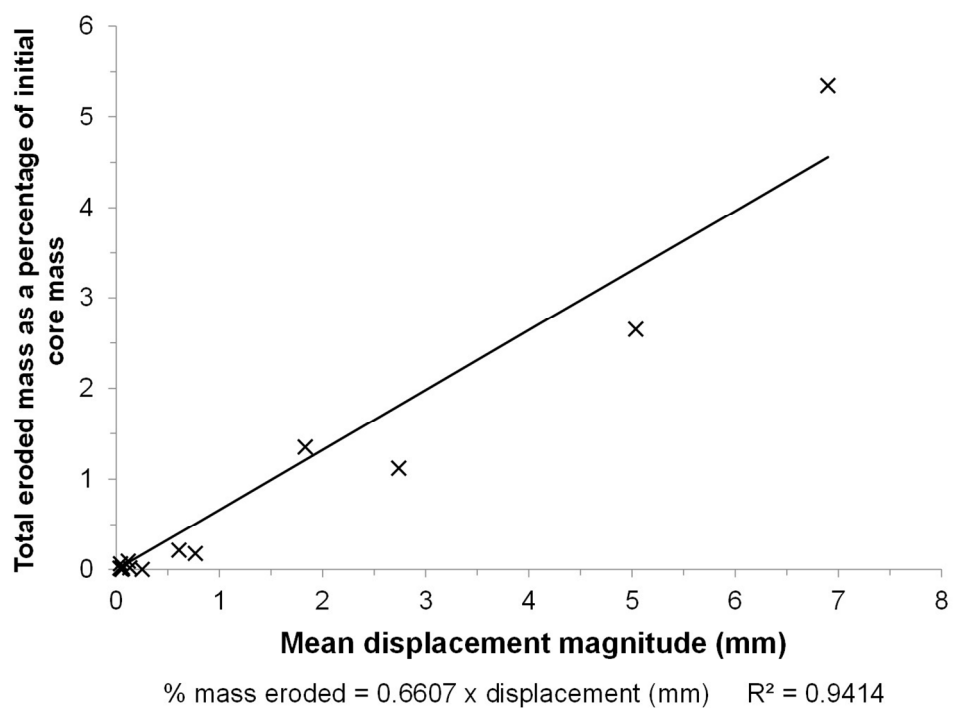


Figure 8: Relationship between mean displacement magnitude and total eroded mass as a percentage of initial core mass

240x174mm (150 x 150 DPI)

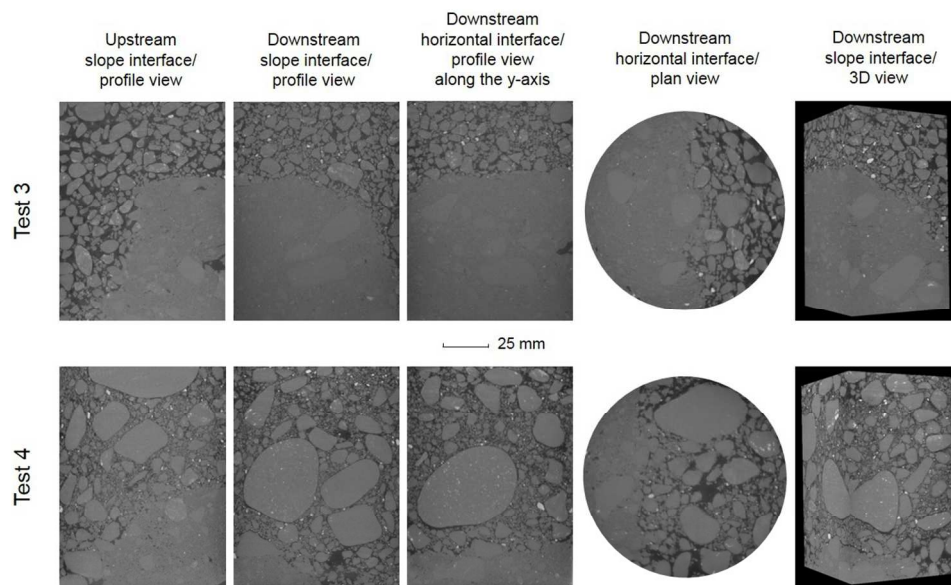


Figure 9:  $\mu$ CT results of downstream and upstream samples for Tests 3 and 4 from different viewpoints  
 225x139mm (150 x 150 DPI)

1

Table 1: Filter criteria, adapted from Fell et al. (2015)

Base soil description	$A$ (%)	Filter criteria
Fine silts and clays	> 85	$D_{15} \leq 9d_{85}$ **
Sands, silts, clays and silty and clayey sands	35 – 85	$D_{15} \leq 0.7 \text{ mm}$
Sands and gravels	< 15	$D_{15} \leq 4d_{85}$
Silty and clayey sands and gravels	15 – 35	$D_{15} \leq \left( \frac{35 - A}{35 - 15} \right) (4d_{85} - 0.7 \text{ mm}) + 0.7 \text{ mm}$ ***

2  
3  
4  
5  
6  
7

\* For a base soil containing particles larger than the No. 4 (4.75 mm) sieve,  $A$  is determined from the gradation curve of the base soil which has been adjusted to 100 % passing the No. 4 (4.75 mm) sieve  
 \*\* When  $9d_{85}$  is less than 0.2 mm, use 0.2 mm  
 \*\*\* When  $4d_{85}$  is less than 0.7 mm, use 0.7 mm

8

Table 2: Filter criteria validation for each test

Core material	<i>A</i> (%)		
Till	36.5		
Test number	Filter material	$D_{15}$ (mm)	Filter criterion fulfillment
1	G1	22	No
2	G2	8	No
3 and 3a	G3	2.5	No
4	2C	0.5	Yes

9

10

11

Table 3: Geotechnical parameters of the materials

Material	Fines content (%)	$C_u$	$D_r$	$e_{min}$	$e_{max}$	$\rho_{d\ min}$ (kg/m <sup>3</sup> )	$\rho_{d\ max}^*$ (kg/m <sup>3</sup> )	$W_{opt}$ (%)
Till	31	19	2.70				2,095	6.75
G1	0	1.5	2.67		0.598	1,671		
G2	0	1.9	2.64		0.576	1,675		
G3	0	3.5	2.68		0.608	1,667		
2C	2	35	2.73	0.205	0.468	1,939	2,266	

12

\*  $\rho_{d\ max}$  was evaluated with ASTM (2012) for the till material and with ASTM (2014a) for 2C material

13

14

15

Table 4: Parameters derived from the compaction state of the materials for each test

Test	Material	$\rho_d$ (kg/m <sup>3</sup> )	$w$ (%)	$e$ (-)	$RC$ (%)	$I_d$ (%)
1	Till	2,033	7.29	0.328	97.0	0
	G1	1,671		0.598		
2	Till	2,034	7.17	0.327	97.1	0
	G2	1,675		0.576		
3 and 3a	Till	2,046	7.12	0.320	97.7	0
	G3	1,667		0.608		
4	Till	2,038	7.18	0.325	97.3	71.2
	2C	2,161		0.268		

16

17

18

Table 5: Eroded dry mass for each upstream water level/cycle of each test

Water level	Test 1 (%)	Test 2 (%)	Test 3 (%)	Test 4 (%)	Cycle	Test 3a (%)
1	0.00	0.00	0.00	0.00	1	$5.64 \times 10^{-3}$
2	5.35*	0.886	$9.19 \times 10^{-3}$	0.00	2	$2.44 \times 10^{-3}$
3		1.07	$4.59 \times 10^{-4}$	0.00	3	$2.76 \times 10^{-3}$
4		0.139	$1.08 \times 10^{-4}$	0.00	4	$2.06 \times 10^{-3}$
5		$3.14 \times 10^{-5}$	0.00	5	$1.90 \times 10^{-3}$	
6		$8.38 \times 10^{-5}$	0.00	6	$2.01 \times 10^{-3}$	
7		$3.13 \times 10^{-4}$	0.00			
8		$6.79 \times 10^{-5}$				
Total**		5.35	2.65	$2.14 \times 10^{-1}$	0.00	

19

20

21

\* Value from this test represents eroded dry mass from levels 2 and 3  
 \*\* Total mass calculation includes the mass eroded that was also collected in the water tank

22

23